CHEMISTRY
A European Journal

www.chemeurj.org

Reprint

A Journal of
ChemPubSoc Europe
ACES
Asian Chemical Editorial Society
WILEY-VCH

ChemPubSoc Europe

DOI: 10.1002/chem.201800840

CHEMISTRY A European Journal Full Paper

Lanthanide Probe

Binding of Lanthanide Complexes to Histidine-Containing Peptides Probed by Raman Optical Activity Spectroscopy

Eva Brichtová,[a, b] Jana Hudecová,[a, c] Nikola Vršková,[a] Jaroslav Šebestík,[a] Petr Bouř,[a, b] and Tao Wu*[a]

Abstract: Lanthanide complexes are used as convenient spectroscopic probes for many biomolecules. Their binding to proteins is believed to be enhanced by the presence of histidine, but the strength of the interaction significantly varies across different systems. To understand the role of peptide length and sequence, short histidine-containing peptides have been synthesized (His-Gly, His-Gly-Gly, His-Gly-Gly-Gly, Gly-His, Gly-His-Gly, His-His, and Gly-Gly-His) and circularly polarized luminescence (CPL) induced at the $[Eu(dpa)_3]^{3-}$ complex has been measured by means of a Raman optical activity (ROA) spectrometer. The obtained data indicate relatively weak binding of the histidine residue to the complex, with a strong participation of other parts of the peptide. Longer peptides, low pH, and a histidine residue close to the *N*-peptide terminus favor the binding. The binding strengths are approximately proportional to the CPL intensity and roughly correlate with predictions based on molecular dynamics (MD) simulations. The specificity of lanthanide binding to the peptide structure and its intense luminescence and high optical activity make the ROA/CPL technique suitable for probing secondary and tertiary structures of peptides and proteins.

Introduction

Luminescent labels of living cell components attract attention because of many applications in analytical biochemistry and imaging.[1] Many of them are based on europium and other lanthanides as these metals exhibit extremely rich luminescence spectra, which are very dependent on the environment.[1g,2] Circularly polarized luminescence (CPL), that is, different emission of left- and right-circularly polarized light, is even more sensitive to the probed structure than the total luminescence (TL) alone.[3]

Lanthanide compounds are thus used to label protein molecules to study their structure, function, and dynamics.[4] Quite often, however, the actual mode of the lanthanide–protein binding is not known, or the interaction is not sufficiently specific. Combinations of lanthanide tags and proteins have therefore been investigated by X-ray crystallography, fluorescence spectroscopy, and NMR spectrometry.[5] Lanthanide CPL can also be used in this context, whereby the chirality in the lanthanide radiation is induced by the environment.[6]

In the present study, we focus on interaction with the histidine residue, which is believed to exhibit exceptional affinity towards heavy metals. Raman optical activity (ROA) spectroscopy has been used to detect TL and CPL. ROA is normally exploited to measure differences in Raman scattering of right- and left-circularly polarized light caused by vibrational transitions.[7] Because the luminescence bands of europium are as narrow as the vibrational bands and appear within the operational range of ROA spectrometers, CPL can be measured as well. In addition, the strong laser radiation source makes it possible to observe quite weak signals, which would be undetectable on more common CPL spectrometers.[8] For example, the strongest Eu^{III} signal that can be measured on our ROA spectrometer is attributable to the $^5D_0 \rightarrow {}^7F_1$ transition[3e,9] and appears as a ("false") Raman band shifted by around 1700–2100 cm^{-1} from the 532 nm laser excitation.

Recently, we showed that CPL spectra of the complex $[Eu(dpa)_3]^{3-}$ offer highly specific insight into the amino acid content of aqueous solutions.[3c] Similar CPL induction has also been observed for a larger protein.[3c] Histidine residues gave rise to a particularly strong signal, most probably because of ion pairing, π-π stacking, and electrostatic interactions between the histidine side chain and the dpa ligand. The dpa complex itself exists in two chiral forms (traditionally referred to as "Λ" and "Δ"), which are normally present in equal amounts. Perturbation of the $\Lambda \rightleftharpoons \Delta$ equilibrium in the presence of a chiral component has been suggested as the primary mechanism of chirality induction, although the presence of more than two spectral components indicates other contribu-

[a] E. Brichtová, J. Hudecová, N. Vršková, Dr. J. Šebestík, Prof. P. Bouř, Dr. T. Wu
Institute of Organic Chemistry and Biochemistry
Academy of SciencesFlemingovo náměstí 2, 16610 Prague (Czech Republic)
E-mail: wu@uochb.cas.cz

[b] E. Brichtová, Prof. P. Bouř
Department of Analytical Chemistry
University of Chemistry and Technology
Technická 5, 16628 Prague (Czech Republic)

[c] J. Hudecová
Faculty of Mathematics and Physics, Institute of Physics
Charles University, Ke Karlovu 5, 12116 Prague (Czech Republic)

Supporting information and the ORCID number(s) for the author(s) of this article can be found under https://doi.org/10.1002/chem.201800840.

tions as well. Other mechanisms of chiral CPL discrimination may include selective luminescence quenching or enhancement, especially for weakly bound complexes.[10]

To better understand the binding mode and the role therein of the main peptide chain, we have synthesized a series of seven histidine-containing model peptides (Figure 1). As a result, we have identified some general trends that provide insight into the interactions between the peptides and the lanthanide probe, which can be at least partially rationalized by molecular dynamics (MD) simulations. In particular, we have correlated the CPL intensity with the binding strength, and have investigated factors affecting the chirality recognition and induction.

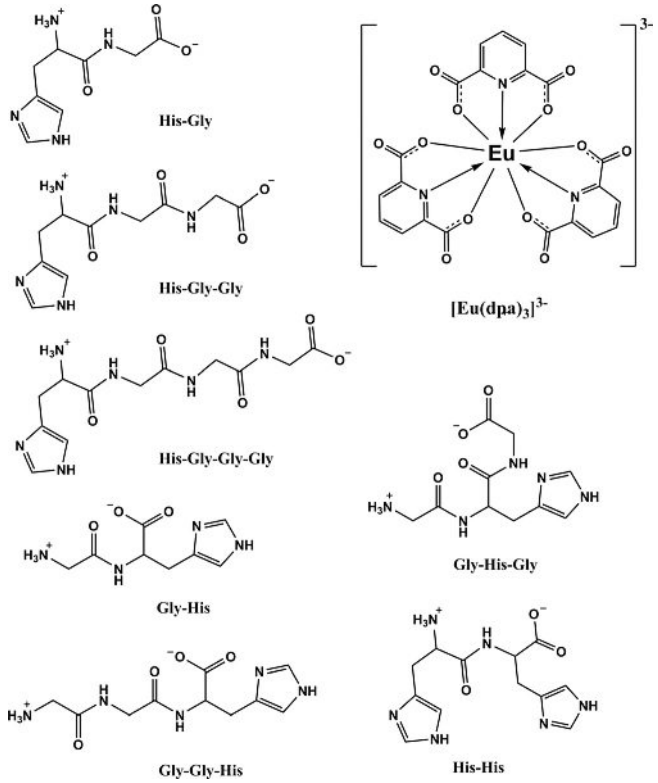

Figure 1. Structures of the $[Eu(dpa)_3]^{3-}$ complex and the investigated model peptides.

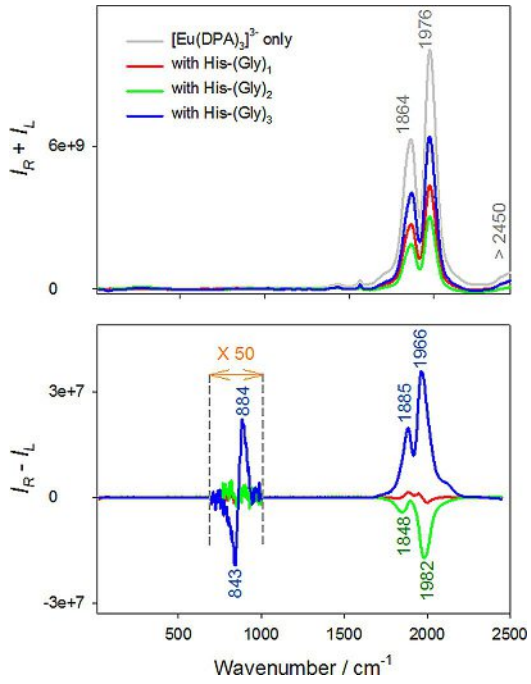

Figure 2. TL and CPL spectra of $[Eu(dpa)_3]^{3-}$ (4 mM) chelated with His-$(Gly)_n$ ($n = 1$, 2, and 3, 20 mM, pH 4).

Table 1. Assignment of observed europium luminescence bands in solutions of $[Eu(dpa)_3]^{3-}$ and His-$(Gly)_n$, Raman shifts from the 532 nm laser frequency (δ, in cm^{-1}), and corresponding wavelengths (λ, in nm).

Transition	$[Eu(dpa)_3]^{3-}$		with His-Gly		with His-$(Gly)_2$		with His-$(Gly)_3$	
	δ	λ	δ	λ	δ	λ	δ	λ
$^5D_0 \rightarrow {}^7F_2$	> 2450	615	> 2450	615	> 2450	615	2400	610
							2263	605
$^5D_0 \rightarrow {}^7F_1$	1976	594	2118	600				
	1864	591	1999	595	1982	595		
			1976	594	1976	594	1976	594
			1950	594			1966	594
			1885	591			1887	591
			1866	591	1866	591	1866	591
			1816	589	1848	590		
$^5D_1 \rightarrow {}^7F_2$			887	558			884	558
			846	557			843	557

Results and Discussion

Effect of peptide length for His-$(Gly)_n$ ($n = 1$, 2, 3)

The TL and CPL spectra obtained for this series of peptides when mixed with $Na_3[Eu(dpa)_3]$ solution at pH 4 are plotted in Figure 2. They are dominated by the strong Eu^{3+} $^5D_0 \rightarrow {}^7F_1$ luminescence band[3c,11] at around 1900 cm^{-1}. A weaker signal at around 850 cm^{-1} can be ascribed to the $^5D_1 \rightarrow {}^7F_2$ transition[11] and is only visible in the differential (CPL) spectrum. On the other hand, invisible in CPL, a TL signal is apparent at the extremity of the spectrometer operational range, close to 2450 cm^{-1}, attributable to the $^5D_0 \rightarrow {}^7F_2$ transition. The center band frequencies are summarized in Table 1. Vibrational Raman and ROA intensities are much weaker than the luminescence and almost undetectable under these conditions.

Addition of the peptides leads to a decrease of around 30–70% in the total luminescence compared to that of the pure $Na_3[Eu(dpa)_3]$ complex. For CPL, the differences are even more dramatic. Only the His-Gly CPL is rather weak at around 1900 cm^{-1} and hidden in noise at 850 cm^{-1}. Note that this may mean that the interaction with the complex is weak and/or does not lead to chiral discrimination. His-$(Gly)_2$ provides a much stronger negative CPL band at 1982 cm^{-1}, a weaker one at 1848 cm^{-1}, and a very weak signal at around 850 cm^{-1}. Judging from the CPL intensities, the interaction with the complex is strongest for the longest His-$(Gly)_3$ peptide, providing

the strongest signal in both the $^5D_0 \rightarrow {}^7F_1$ and $^5D_1 \rightarrow {}^7F_2$ regions. However, the $^5D_0 \rightarrow {}^7F_1$ bands have nearly opposite sign compared to those of His-$(Gly)_2$. Although the CPL shapes for His-$(Gly)_2$ and His-$(Gly)_3$ are not exact "mirror images", as a first approximation we may interpret the results in terms of perturbation of the $\Lambda \rightleftharpoons \Delta$ complex enantiomeric equilibrium by the chiral peptide matrices.[12] For His-$(Gly)_3$, the absolute CPL intensity is greater than that for His-$(Gly)_2$, as is the ratio of the polarized and total luminescences ($CID = 5.0 \times 10^{-3}$ at 1976 cm^{-1}). *CID* values for other systems at selected wavenumbers are listed in Table 2.

Table 2. *CID* (CPL/TL) ratios for the bands at 1976 and 1864 cm^{-1} ($^5D_0 \rightarrow {}^7F_1$) of $[Eu(dpa)_3]^{3-}$–peptide complexes.

Peptide	CID	
	1976 cm^{-1}	1864 cm^{-1}
His-Gly	-9.1×10^{-5}	2.3×10^{-4}
His-$(Gly)_2$	-4.1×10^{-3}	-1.2×10^{-3}
His-$(Gly)_3$	5.0×10^{-3}	3.2×10^{-3}
Gly-His	1.6×10^{-3}	7.6×10^{-4}
Gly-His-Gly	2.7×10^{-3}	1.3×10^{-3}
Gly-Gly-His	2.2×10^{-3}	8.8×10^{-4}
His-His	6.3×10^{-3}	3.8×10^{-3}

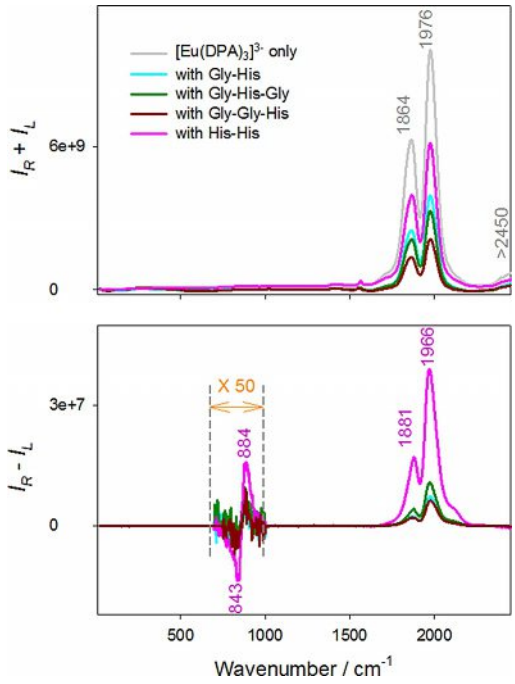

Figure 3. TL and CPL spectra of $[Eu(dpa)_3]^{3-}$ (4 mM) chelated with Gly-His, Gly-His-Gly, Gly-Gly-His, and His-His (each 20 mM, pH 4).

Note that, using the ROA terminology, we measure the ratio as the circular intensity difference, $CID = (I_R - I_L)/(I_R + I_L)$, where I_R and I_L are the intensities of the right and left circularly polarized light, respectively. In CPL spectroscopy, the dissymmetry factor is often used instead, $g = 2(I_L - I_R)/(I_L + I_R)$, that is, $CID = -g/2$.

To summarize, the longer peptide binds the europium complex much better than the shorter ones, that is, parts other than the histidine residues are also important for the binding, and the chirality discrimination and induction is determined by the peptide as a whole, not only by the L-histidine moiety.

Position of the histidine in the peptide chain: Gly-His, Gly-His-Gly, Gly-Gly-His, and His-His

Interestingly, few prominent spectral differences are apparent within this series of peptides (Figure 3). As before, the total luminescence of the complex is partially quenched, but only one-sign CPL in the region 1700–2000 cm^{-1} appears upon mixing with the peptides. Nevertheless, the spectra do exhibit significant differences, allowing discrimination between different peptide species. His-His clearly provides the strongest CPL signal and a large *CID* (6.3×10^{-3}, Table 2), which confirms the importance of the histidine residue for binding. The other three peptides of this series provide rather weak CPL, although with comparable *CID* ratios (*CID*s as functions of the wavenumber over a broader range are plotted in Figure S1).

Compared to His-$(Gly)_2$ from the previous series, placing the histidine residue in the middle (Gly-His-Gly) or at the C-terminus (Gly-Gly-His) induces the opposite CPL sign for the $^5D_0 \rightarrow {}^7F_1$ signal. The latter two peptides most probably stabilize the opposite enantiomer of the complex, but the binding strengths, as judged from the absolute *CID* ratios, are weaker. As for the CPL, in the sequence His-Gly-Gly, Gly-His-Gly, and Gly-Gly-His, the total luminescence intensity gradually decreases. We can speculate that in His-$(Gly)_2$ the NH_3^+ charge strengthens the binding potency of histidine, whereas in Gly-His-Gly and Gly-Gly-His the C-terminal COO^- group weakens it. This concept is seemingly not applicable for the His-Gly and Gly-His pairs, both providing weak CPL, although this may be caused by a strong, but not chirality-sensitive interaction. Other factors, such as dissociation equilibria and van der Waals interactions, are also likely to contribute to the electrostatic effects. One also has to realize that "binding" is in all cases very weak and the resultant assembly may not have a rigid geometry.[3b] Strong complexation of europium with a product of fixed geometry would have led to much larger *CID* values than those observed in the present study, up to the order of one.[8a]

CPL of the $^5D_1 \rightarrow {}^7F_2$ transition (around 850 cm^{-1}) is consistent with the results for the main $^5D_0 \rightarrow {}^7F_1$ bands in that the sign pattern does not change in the second series of peptides, and the "$-/+$" couplet shape (if viewed from lower to higher wavenumbers) always accompanies the positive $^5D_0 \rightarrow {}^7F_1$ signal.

pH dependence of the spectra

As has been previously shown for individual amino acids, the predominantly positive charge of the peptides at pH 4 favors the interaction with the complex.[3c] Indeed, the TL and CPL spectra induced by His-Gly, His-$(Gly)_2$, and His-$(Gly)_3$ at three pH values (4, 7, and 10), as plotted in Figure S2, document that the interaction is significantly weakened at higher pH.

More detailed inspection reveals further differences, which may allow better understanding of the interaction with the complex. The CPL intensity of His-Gly, which is already weak at pH 4, further decreases to about 20% (at 1885 cm^{-1}) at pH 7, and changes sign at pH 10. This confirms that the electrostatic interaction itself is not solely responsible for the chirality induction. For the (relatively) strong binders His-$(Gly)_2$ and His-$(Gly)_3$, the situation is simpler in that the CPL more or less vanishes at higher pH. Moreover, at the two higher pH values, no CPL is observed for the $^5D_0 \rightarrow {}^7F_2$ ($>2200\ cm^{-1}$) and $^5D_1 \rightarrow {}^7F_2$ ($\approx 850\ cm^{-1}$) transitions. The total luminescence remaining about constant at pH 7 and 10, but decreasing by about 30–60% at pH 4, is more consistently observed within the three peptides than the CPL.

We verified that, under the experimental conditions employed (pH > 4), the luminescence of the pure $[Eu(dpa)_3]^{3-}$ complex does not change. However, slight dissociation may still occur at around pH 4,[13] which could also contribute to the observed changes, such as the decrease in TL at low pH (Figure S2).

Titration curves

So far, spectra obtained at 5:1 peptide/complex ratios have been reported, around which signals are maximized. TL and CPL intensities obtained for different ratios of the complex and His-$(Gly)_2$ and His-His peptides, as plotted in Figure S3, confirm that the interaction is rather weak, because the titrations cause only gradual changes in the spectra. As an alternative view, maximum Raman, ROA, and *CID* intensities at 1976 cm^{-1} are plotted in Figure 4. It can be seen that the spectral intensities do not stabilize at higher peptide concentrations, that is to say, the dependences differ from "classical" two-system titration curves. Instead, the Raman intensities almost exponentially vanish with increasing peptide concentrations, while the ROA/*CID* values exhibit maxima at optimal peptide–complex ratios of around 4–7. One may speculate that more peptide molecules become bonded to the complex; however, the actual cause of the concentration dependence will likely be quite complicated, including luminescence quenching by the peptide[2b] and possible binding and decomposition of the complex by peptide impurities (mostly trifluoroacetic acid from the synthesis) at very high peptide concentrations.

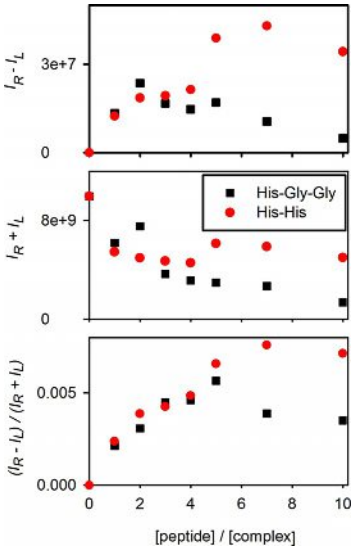

Figure 4. Dependences of the maximal Raman, ROA, and *CID* signals (at 1976 cm^{-1}) on the peptide/complex molar ratio.

Theoretical analysis

In spite of the complexity of the lanthanide complex–peptide interactions, molecular dynamics simulation can provide at least a qualitative understanding of the observed data. Calculated dependences of the free energy on the $[Eu(dpa)_3]^{3-}$–$His(Gly)_n$ distance (between Eu and $^{\alpha}C$ of His) are plotted in Figure 5. Free-energy profiles for the other peptides at other pH values were fairly similar (Figures S4 and S5). The stabilization energies are rather low (ca. 2 kcal mol^{-1}), corresponding to the experimental observations, in particular the nonspecific titration curves discussed above. For His-Gly and His-$(Gly)_2$, no favoring of the Λ or Δ enantiomer within computational accuracy is apparent. For His-$(Gly)_3$, however, the Δ binding seems to be more energetically favorable than that of the Λ form. Thus, the simulation does not readily reproduce the chirality inversion observed for His-$(Gly)_2$ and His-$(Gly)_3$, but does corroborate the stronger binding observed for His-$(Gly)_3$.

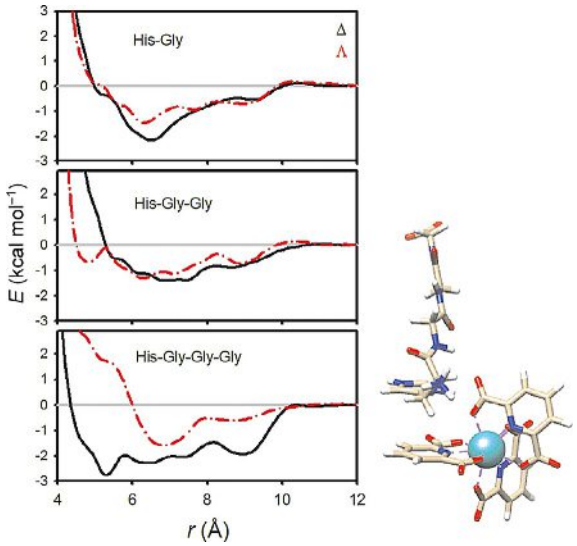

Figure 5. Dependence of the calculated free energy on the Eu–His-$(Gly)_n$ peptide distance corresponding to pH ≈ 4, and example of an energy-minimized structure for His-$(Gly)_3$.

In all cases, however, the energy "well" is quite broad and shallow. Inspection of geometries obtained close to the energy minima (such as the structure in Figure 5) suggests a significant role of the histidine charge and perhaps a π-π interaction of the histidine ring with the ligand of the complex. In some MD snapshots, interaction of the glycine residues with the complex is also apparent, which is consistent with the relatively high CPL observed for the longest His-$(Gly)_3$ peptide.

Binding strengths, as defined on the basis of the MD simulations, are compared for more peptides and pH values in Figure 6. The environmental pH (2, 4, 7, and 10) was simulated by different charges on the peptides (+2, +1, 0, and −1, respectively). At around pH 4 (charge +1), for example, the computation predicts strong binding for His-$(Gly)_3$ and His-His, nicely corroborating the data in Figures 2 and 3. In addition, the Δ form of the complex is most stabilized, which again is most probably reflected in the same CPL sign.

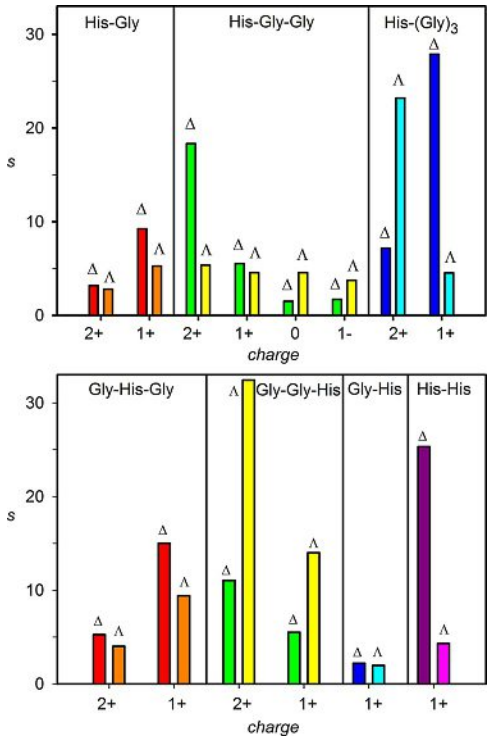

Figure 6. Calculated binding strengths of the peptides *s*, obtained as the ratio (N_B/N_F) of bonded and free complex molecules in the simulation box.

As noted above, the CPL chirality inversion observed for His-$(Gly)_2$ and His-$(Gly)_3$ is not unambiguously supported theoretically; nevertheless, it can be seen that at pH 4 the Λ and Δ forms of His-$(Gly)_2$ are predicted to be adopted with about the same probability, whereas at higher pH the Λ form is preferred. The inversion can thus be at least partially explained by a residual presence of the neutral species in the sample. However, the theoretical preference for the Λ enantiomer of Gly-Gly-His is inconsistent with the observations. Thus, the simulations at the present level do not seem to be sufficiently reliable to be applied for chirality determination. Nevertheless, they adequately explain many aspects of the binding, including some general trends, and at least suggest that the quite attractive idea of determination of the absolute configuration of a complex through a combination of theory and experiment is possible.

Conclusions

We have synthesized a series of histidine-containing peptides and have monitored their interactions with a racemic Eu^{III} complex through circularly polarized luminescence measurements. The results show that both the length of the peptides and the histidine position therein profoundly affect the binding modes. The acquired data could be very well rationalized by molecular dynamics simulations, although these were not sufficiently accurate to unambiguously provide the absolute configurations of the preferred complex forms. The data and simulation indicate that the interaction of the complex with the peptides is rather weak and non-site-specific in terms of interaction energies and product geometries, although the resultant luminescence and CPL patterns are still quite characteristic for individual peptides. This is promising for future design of similar "smart" probes of peptide, protein, and other biomolecular structures.

Experimental Section

Synthesis: $Na_3[Eu(dpa)_3]$ (dpa = dipicolinate = 2,6-pyridinedicarboxylate; Figure 1) was obtained by the reaction of europium(III) carbonate and pyridine-2,6-dicarboxylic acid (1:3 molar ratio) in water; pH 7 was adjusted with 1 M sodium carbonate solution.[3c] The peptides were synthesized by the Fmoc/*t*Bu strategy on 2-chlorotrityl resin. The volume to mass ratio of the agent solution to the 2-chlorotrityl resin was 10 mL g^{-1}. The synthesized peptides were then cleaved with a 20% solution of 2,2,2-trifluoroethanol in CH_2Cl_2; the trityl group protecting the histidine side chain was cleaved with a mixture of TFA, triisopropylsilane (TIS), and water (9.5:2.5:2.5, v/v). The volatiles were then removed by evaporation, and the residual solid was dissolved in water. Insoluble by-products were removed by filtration. Water was evaporated and the peptide products were recovered by a combination of vacuum evaporation and lyophilization. The products were characterized by TLC on silica-gel-coated aluminum plates, whereby the compounds were visualized by ninhydrin spraying. ^1H and ^{13}C NMR spectra were measured at ambient temperature from solutions in 5 mm diameter NMR tubes (see the Supporting Information for further details).

CPL measurement: Back-scattering Raman and scattered circular polarization (SCP) ROA spectra (dominated by Eu TL and CPL) were acquired on a BioTools ROA spectrometer operating with laser excitation at 532 nm and a resolution of 7 cm^{-1}. For the lanthanide CPL measurement, the laser power at the sample was 150–400 mW, and accumulation times were 1 h (for solutions at pH 4), 8 h (pH 7), or 12 h (pH 10). pH was adjusted with 0.1 M HCl or NaOH. Concentrations were 20 mM for peptides and 4 mM for the $[Eu(dpa)_3]^{3-}$complex. In the presented spectra, the intensities were normalized to the 1650 cm^{-1} band, and a broad luminescence background attributable to sample impurities was subtracted from the Raman signal.

Computations: The initial geometry of the $[Eu(dpa)_3]^{3-}$ complex was obtained using the Gaussian 09 program,[14] adopting the B3LYP functional and the 6-31G(d,p) basis set (MWB28 pseudopotential and basis set for Eu). By titration, we found that the $Na_3[Eu(dpa)_3]$ CPL spectra do not change within the interval pH 4–12. We therefore suppose that the charge (−3) of the complex is not changed in our experiments. The solvent was modeled by the conductor-like polarizable continuum solvent model (CPCM).[15]

The interactions of all seven peptides (Figure 1) with the Λ and Δ forms of the complex in aqueous solution were investigated using Amber 14[16] MD software. To model mild acidic conditions (pH ≈ 4, corresponding to most experiments), the histidine aromatic ring and the amine group were protonated (-NH_3^+) and the carboxyl group was deprotonated (-COO^-). For lower pH (< 2), the carboxyl group (-COOH) was also protonated, and for His-$(Gly)_2$ the neutral and basic forms were considered as zwitterionic and deprotonated peptides. For the other peptides, only structures corresponding to acidic conditions (pH < 2 and pH ≈ 4, with peptide charges of +2 and +1, respectively) were investigated. The peptides were inserted into a cubic $(30\ Å)^3$ box containing 880 water molecules and one $[Eu(dpa)_3]^{3-}$ ion, initially separated from the peptide by about 12 Å. Separate simulations were performed for the Λ and Δ forms of the complex. MD simulations were run for *NVT* ensembles using a 1 fs integration step, a temperature of 300 K, and GAFF[17] (dpa ligands), Amber 14SB[18] (His and Gly), or TIP3P6[19] (water) force fields.

After an equilibration (1 ns), constrained MD simulations were run for 8 ns. A harmonic penalty function (restraint constant of 4 kcal $Å^{-2}\,mol^{-1}$) was applied to the distance (r) between the europium atom of the complex and C^α of histidine; the distance was changed from 12 to 9 Å in 1 Å increments and from 9 and 4 Å in 0.5 Å increments. From individual distance distributions, the potential of the mean force $F(r)$ was calculated by the weighted histogram analysis method (WHAM)[20] using the Amber 14 scripts.

The simulations indicated rather weak peptide–complex associates with flexible geometries. Therefore, to better evaluate effective relative binding strengths (s), equilibrium ratios of the numbers of bonded (N_B, $r < 10$ Å) and free (N_F, $r > 10$ Å) europium complexes for each box were calculated as $s = N_B/N_F = \int_0^{10} \exp(-F/kT) r^2 dr / \int_{10}^{12} \exp(-F/kT) r^2 dr$.

Acknowledgements

This work was supported by the Czech Science Foundation (16-08764Y and 18-05770S), the Ministry of Education (LTC17012/CA15214), and CESNET (LM2015042) and CERIT (LM2015085) computational resources.

Conflict of interest

The authors declare no conflict of interest.

Keywords: biomolecular probe · chemical imaging · circularly polarized luminescence · histidine · lanthanide-binding peptide · molecular dynamics · Raman optical activity · rare earths

[1] a) J. C. G. Bünzli, *J. Lumin.* **2016**, *170*, 866–878; b) S. M. J. van Duijnhoven, M. S. Robillard, S. Langereis, H. Grul, *Contrast Media Mol. Imaging* **2015**, *10*, 282–308; c) A. S. Klymchenko, *Acc. Chem. Res.* **2017**, *50*, 366–375; d) G. Kramer-Marek, M. R. Longmire, P. L. Choyke, H. Kobayashi, *Curr. Med. Chem.* **2012**, *19*, 4759–4766; e) J. C. G. Bünzli, *Chem. Rev.* **2010**, *110*, 2729–2755; f) U. Resch-Genger, M. Grabolle, S. Cavaliere-Jaricot, R. Nitschke, T. Nann, *Nat. Methods* **2008**, *5*, 763–775; g) M. C. Heffern, L. M. Matosziuk, T. J. Meade, *Chem. Rev.* **2014**, *114*, 4496–4539.

[2] a) M. Sy, A. Nonat, N. Hildebrandt, L. J. Charbonniere, *Chem. Commun.* **2016**, *52*, 5080–5095; b) S. Shuvaev, M. Starck, D. Parker, *Chem. Eur. J.* **2017**, *23*, 9974–9989.

[3] a) T. Wu, J. Kapitán, V. Andrushchenko, P. Bouř, *Anal. Chem.* **2017**, *89*, 5043–5049; b) T. Wu, J. Průša, J. Kessler, D. Dračínský, J. Valenta, P. Bouř, *Anal. Chem.* **2016**, *88*, 8878–8885; c) T. Wu, J. Kessler, P. Bouř, *Phys. Chem. Chem. Phys.* **2016**, *18*, 23803–23811; d) E. R. Neil, D. Parker, *RSC Adv.* **2017**, *7*, 4531–4540; e) F. Zinna, L. Di Bari, *Chirality* **2015**, *27*, 1–13; f) E. M. Sánchez-Carnerero, A. R. Agarrabeitia, F. Moreno, B. L. Maroto, G. Muller, M. J. Ortiz, S. de la Moya, *Chem. Eur. J.* **2015**, *21*, 13488–13500; g) J. Kumar, T. Nakashima, T. Kawai, *J. Phys. Chem. Lett.* **2015**, *6*, 3445–3452; h) J. P. Riehl, G. Muller, *Circularly Polarized Luminescence Spectroscopy and Emission-Detected Circular Dichroism*, Wiley, Hoboken, **2012**.

[4] a) J. Veliscek-Carolan, T. L. Hanley, K. A. Jolliffe, *RSC Adv.* **2016**, *6*, 75336–75346; b) L. Ancel, A. Niedzwiecka, C. Lebrun, C. Gateau, P. Delangle, *C. R. Chim.* **2013**, *16*, 515–523; c) J. A. González-Vera, *Chem. Soc. Rev.* **2012**, *41*, 1652–1664.

[5] a) K. Barthelmes, A. M. Reynolds, E. Peisach, H. R. A. Jonker, N. J. DeNunzio, K. N. Allen, B. Imperiali, H. Schwalbe, *J. Am. Chem. Soc.* **2011**, *133*, 808–819; b) K. N. Allen, B. Imperiali, *Curr. Opin. Chem. Biol.* **2010**, *14*, 247–254.

[6] a) G. Muller, *Dalton Trans.* **2009**, 9692–9707; b) R. Carr, N. H. Evans, D. Parker, *Chem. Soc. Rev.* **2012**, *41*, 7673–7686.

[7] a) T. Wu, X. Z. You, P. Bouř, *Coord. Chem. Rev.* **2015**, *284*, 1–18; b) L. D. Barron, *Biomed. Spectrosc. Imaging* **2015**, *4*, 223–253.

[8] a) T. Wu, J. Kapitán, V. Mašek, P. Bouř, *Angew. Chem. Int. Ed.* **2015**, *54*, 14933–14936; *Angew. Chem.* **2015**, *127*, 15146–15149; b) T. Wu, P. Bouř, *Chem. Commun.* **2018**, *54*, 1790–1792.

[9] F. S. Richardson, *Inorg. Chem.* **1980**, *19*, 2806–2812.

[10] a) J. Yuasa, T. Ohno, H. Tsumatori, R. Shiba, H. Kamikubo, M. Kataoka, Y. Hasegawa, T. Kawai, *Chem. Commun.* **2013**, *49*, 4604–4606; b) M. Leonzio, A. Melchior, G. Faura, M. Tolazzi, M. Bettinelli, F. Zinna, L. Arrico, L. Di Bari, F. Piccinelli, *New. J. Chem.* DOI: https://doi.org/10.1039/c7nj04640e.

[11] K. Binnemans, *Coord. Chem. Rev.* **2015**, *295*, 1–45.

[12] a) A. Moussa, C. Pham, S. Bommireddy, G. Muller, *Chirality* **2009**, *21*, 497–506; b) J. C. G. Bünzli, C. Piguet, *Chem. Soc. Rev.* **2005**, *34*, 1048–1077; c) G. Muller, F. C. Muller, C. L. Maupin, J. P. Riehl, *Chem. Commun.* **2005**, 3615–3617.

[13] G. Jones, V. I. Vullev, *J. Phys. Chem. A* **2002**, *106*, 8213–8222.

[14] Gaussian 09 (Revision D.01), M. J. Frisch, G. W. Trucks, H. B. Schlegel, G. E. Scuseria, M. A. Robb, J. R. Cheeseman, G. Scalmani, V. Barone, B. Mennucci, G. A. Petersson, H. Nakatsuji, M. Caricato, X. Li, H. P. Hratchian, A. F. Izmaylov, J. Bloino, G. Zheng, J. L. Sonnenberg, M. Hada, M. Ehara, K. Toyota, R. Fukuda, J. Hasegawa, M. Ishida, T. Nakajima, Y. Honda, O. Kitao, H. Nakai, T. Vreven, J. A. Montgomery, Jr., J. E. Peralta, F. Ogliaro, M. Bearpark, J. J. Heyd, E. Brothers, K. N. Kudin, V. N. Staroverov, R. Kobayashi, J. Normand, K. Raghavachari, A. Rendell, J. C. Burant, S. S. Iyengar, J. Tomasi, M. Cossi, N. Rega, J. M. Millam, M. Klene, J. E. Knox, J. B. Cross, V. Bakken, C. Adamo, J. Jaramillo, R. Gomperts, R. E. Stratmann, O. Yazyev, A. J. Austin, R. Cammi, C. Pomelli, J. W. Ochterski, R. L. Martin, K. Morokuma, V. G. Zakrzewski, G. A. Voth, P. Salvador, J. J. Dannenberg, S. Dapprich, A. D. Daniels, O. Farkas, J. B. Foresman, J. V. Ortiz, J. Cioslowski, D. J. Fox, Gaussian Inc., Wallingford CT, **2013**.

[15] A. Klamt, *J. Phys. Chem.* **1995**, *99*, 2224–2235.

[16] D. A. Pearlman, D. A. Case, J. W. Caldwell, W. S. Ross, T. E. Cheatham, S. Debolt, D. Ferguson, G. Seibel, P. Kollman, *Comput. Phys. Commun.* **1995**, *91*, 1–41.

[17] J. Wang, R. M. Wolf, J. W. Caldwell, P. A. Kollman, D. A. Case, *J. Comput. Chem.* **2005**, *25*, 1157–1174.

[18] J. A. Maier, C. Martinez, K. Kasavajhala, L. Wickstrom, K. E. Hauser, C. Simmerling, *J. Chem. Theory Comput.* **2015**, *11*, 3696–3713.

[19] W. L. Jorgensen, J. Chandrasekhar, J. D. Madura, *J. Chem. Phys.* **1983**, *79*, 926–935.

[20] a) S. Kumar, D. Bouzida, R. H. Swendsen, P. A. Kollman, J. M. Rosenberg, *J. Comput. Chem.* **1992**, *13*, 1011–1021; b) B. Roux, *Comput. Phys. Commun.* **1995**, *91*, 275–282.

Manuscript received: February 18, 2018
Accepted manuscript online: April 14, 2018
Version of record online: May 22, 2018